Chapter 14

The Atlantic Ocean

A glance at the distribution of high quality ocean data (Figure 2.3) tells us that the Atlantic Ocean is by far the best researched part of the world ocean. This is particularly true of the North Atlantic Ocean, the home ground of many oceanographic research institutions of the USA and Europe. We therefore have a wealth of information, and our task in describing the essential features of the Atlantic Ocean will not so much consist of finding reasonable estimates for missing data but finding the correct level of generalization from a bewildering and complex data set.

Bottom topography

Several outstanding topographic features distinguish the Atlantic Ocean from the Pacific and Indian Oceans. First of all, the Atlantic Ocean extends both into the Arctic and Antarctic regions, giving it a total meridional extent - if the Atlantic part of the Southern Ocean is included - of over 21,000 km from Bering Strait through the Arctic Mediterranean Sea to the Antarctic continent. In comparison, its largest zonal distance, between the Gulf of Mexico and the coast of north west Africa, spans little more than 8,300 km. Secondly, the Atlantic Ocean has the largest number of adjacent seas, including mediterranean seas which influence the characteristics of its waters. Finally, the Atlantic Ocean is divided rather equally into a series of eastern and western basins by the Mid-Atlantic Ridge, which in many parts rises to less than 1000 m depth, reaches the 2000 m depth contour nearly everywhere, and consequently has a strong impact on the circulation of the deeper layers.

When all its adjacent seas are included, the Atlantic Ocean covers an area of $106.6 \cdot 10^6$ km^2. Without the Arctic Mediterranean and the Atlantic part of the Southern Ocean, its size amounts to $74 \cdot 10^6$ km^2, slightly less than the size of the Southern Ocean. Although all its abyssal basins are deeper than 5000 m and most extend beyond 6000 m depth in their deepest parts (Figure 14.1), the average depth of the Atlantic Ocean is 3300 m, less than the mean depths of both the Pacific and Indian Oceans. This results from the fact that shelf seas (including its adjacent and mediterranean seas) account for over 13% of the surface area of the Atlantic Ocean, which is two to three times the percentage found in the other oceans.

Three of the features shown in Figure 14.1 deserve special mention. The first is the difference in depth east and west of the Mid-Atlantic Ridge near 30°S. The Rio Grande Rise comes up to about 650 m; but west of it the Rio Grande Gap allows passage of deep water near the 4400 m level. In contrast, the Walvis Ridge in the east, which does not reach 700 m depth, blocks flow at the 4000 m level. The second is the Romanche Fracture Zone (Figure 8.2) some 20 km north of the equator which allows movement of water between the western and eastern deep basins at the 4500 m level (its deepest part, the Romanche Deep, exceeds 7700 m depth but connects only to the western basins). Other fracture zones north of the equator have similar characteristics; but the Romanche Fracture Zone is the first opportunity for water coming from the south to break through the barrier posed by the Mid-Atlantic Ridge. The third feature is the Gibbs Fracture Zone near 53°N which allows passage of water at the 3000 m level; its importance for the spreading of Arctic Bottom Water was already discussed in Chapter 7.
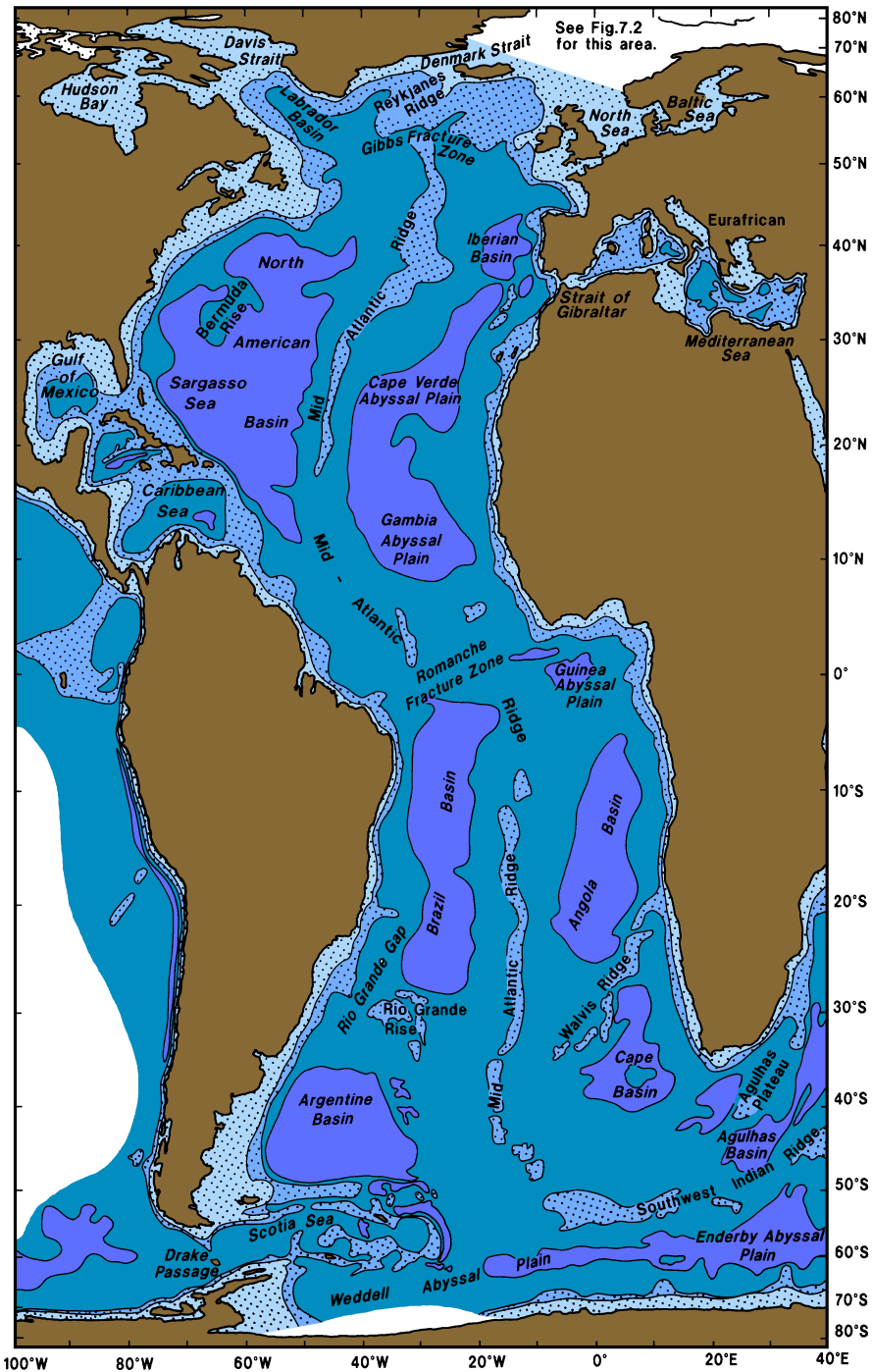
Fig. 14.1. Topography of the Atlantic Ocean. The 1000, 3000, and 5000 m isobaths are shown, and regions less than 3000 m deep are shaded.

Of interest from the point of view of oceanography are the sill characteristics of the five mediterranean seas. The Arctic Mediterranean Sea, which is by far the largest comprising 13% of the Atlantic Ocean area, was already discussed in Chapter 7; its sill is about 1700 km wide and generally less than 500 m deep with passages exceeding 600 m depth in Denmark Strait and 800 m in the Faroe Bank Channel. The Strait of Gibraltar, the point of communication between the Eurafrican Mediterranean Sea and the main Atlantic Ocean, spans a distance of 22 km with a sill depth of 320 m. The American Mediterranean Sea has several connections with the Atlantic Ocean basins, the major ones being east of Puerto Rico and between Cuba and Haiti where sill depths are in the vicinity of 1700 m and between Florida and the Bahamas with a sill depth near 750 m. Baffin Bay communicates through the 350 km wide Davis Strait where the sill depth is less than 600 m. Finally, communication with the Baltic Sea is severely restricted by the shallow and narrow system of passages of Skagerrak, Kattegat, Sund and Belt where the sill depth is only 18 m.

The wind regime

The information needed from the atmosphere is again included in Figures 1.2 - 1.4. An outstanding feature is the large seasonal variation of northern hemisphere winds in comparison to the low variability of the wind field in the subtropical zone of the southern hemisphere. This is similar to the situation in the Pacific Ocean and again caused by the impact of the Siberian and to a lesser extent North American land masses on the air pressure distribution. As a result the subtropical high pressure belt, which in the northern winter runs from the Florida - Bermuda region across the Canary Islands, the Azores, and Madeira and continues across the Sahara and the Eurafrican Mediterranean Sea into central Siberia, is reduced during summer to a cell of high pressure with its centre near the Azores. This is the well-known Azores High which dominates European summer weather, bringing winds of moderate strength. During winter, the contrast between cold air over Siberia and air heated by the advection of warm water in the Norwegian Current region leads to the development of the equally well-known Icelandic Low with its strong Westerlies, which follow the isobars between the subtropical high pressure belt and the low pressure to the north. The seasonal disturbance of the subtropical high pressure belt in the southern hemisphere is much less developed, and the Westerlies show correspondingly less seasonal variation there.

The Trade Winds are somewhat stronger in winter (February north of the equator and August in the south) than in summer on both hemispheres. Seasonal wind reversals of monsoon characteristics are of minor importance in the Atlantic Ocean; their occurrence is limited to two small regions, along the African coastline from Senegal to Ivory Coast and in the Florida - Bermuda area. Important seasonal change in wind direction is observed along the east coast of North America which experiences offshore winds during most of the year but warm alongshore winds in summer.

The mean wind stress distribution of the South Atlantic Ocean shows close resemblance to that of the Indian Ocean. The maximum Westerlies do not lie quite so far north as in the Indian Ocean (at about 50°S instead of 45°S), but the maximum Trade Winds occur at very similar latitudes (about 15°S, associated with somewhat smaller wind stress curls). The Doldrum belt, or Intertropical Convergence Zone (ITCZ), is found north of the equator,

rather like the North Pacific ITCZ but not as accurately zonal; its annual mean position angles from the equator off Brazil to about 7°N off Sierra Leone.

North of the ITCZ the mean wind stress distribution more closely resembles that of the North Pacific Ocean, though the Atlantic Northeast Trades are not quite as strong in comparison. Their maximum strength is at about 15°N. The North Atlantic Westerlies enter the ocean from the northwest, similar to the North Pacific Westerlies. They bring cold, dry air out over the Gulf Stream, just as the Pacific winds bring cold dry air from Siberia out over the Kuroshio. As their Pacific counterpart, the Atlantic Westerlies veer round to a definite southwesterly direction in the eastern Atlantic Ocean, and the axis of maximum westerly strength is also oriented along a line running east-north-east. The polar Easterlies of the Arctic region are more vigorous in the Atlantic than in any other ocean.

The integrated flow

When the Sverdrup balance was introduced and tested in Chapter 4 we noted that the largest discrepancies between the integrated flow fields deduced from wind stress and CTD data are found in the Atlantic Ocean. We now go back to Figure 4.4 and Figures 4.5 or 4.6 for a more detailed comparison, keeping in mind that with the exception of the Southern Ocean, the CTD-derived flow pattern should describe the actual situation quite well. The largest discrepancy between the two flow fields occurs south of 34°S; it was discussed in Chapters 4 and 11. North of 34°S, the subtropical gyres of both hemispheres are well reproduced from both atmospheric and oceanic data, as in the other oceans. To be more specific, the gradient of depth-integrated steric height across the North and South Equatorial Currents is calculated fairly well from both data sets, and the gradient across the equator in the Atlantic seen in the CTD-derived pattern (one contour crosses the equator; P increases westward, as in the Pacific Ocean) also occurs in the wind-calculated pattern (even though no contour happens to cross the equator in this case). That this must be so is evident by inspection of Figure 1.2 which shows weak mean westerly winds along the equator in the Atlantic Ocean; hence the only term on the right hand side of eqn (4.7) at the equator is negative, and P must increase towards the west. However, the agreement between Figures 4.4 and 4.5 or 4.6 is not as good in the Atlantic as in the other oceans. The major reason for this is the recirculation of North Atlantic Deep Water, which was mentioned already in Chapter 7 and will be further discussed Chapter 15. It makes the assumption of a depth of no motion less acceptable than in the other oceans. The transport of thermocline water from the Indian into the Atlantic Ocean which is part of the North Atlantic Deep Water recirculation is also not included in the flow pattern derived from wind data.

In the region where the two circulation patterns compare well, the Sverdrup relation reveals the existence of strong subtropical gyres in both hemispheres and a weaker subpolar gyre in the northern hemisphere. The gyre boundaries coincide reasonably well with the contour of zero curl(t/f) (Figure 4.3). The northern subtropical gyre consists (Figure 14.2) of the North Equatorial Current with its centre near 15°N, the Antilles Current east of, and the Caribbean Current through the American Mediterranean Sea, the Florida Current, the Gulf Stream, the Azores Current, and the Portugal and Canary Currents. The southern gyre is made up of the South Equatorial Current which is centred in the southern hemisphere but extends just across the equator, the Brazil Current, the South Atlantic Current, and the
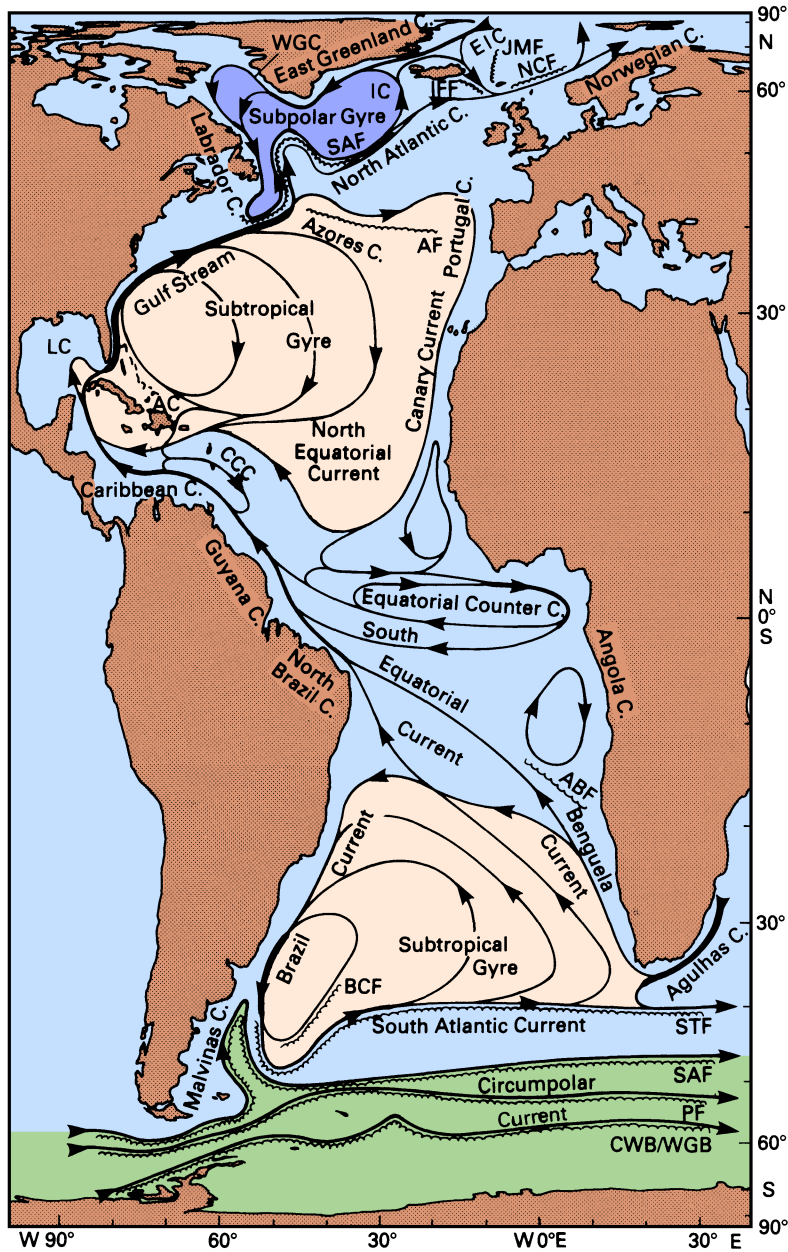
Fig. 14.2. Surface currents of the Atlantic Ocean. Abbreviations are used for the East Iceland (EIC), Irminger (IC), West Greenland (WGC), and Antilles (AC) Currents and the Caribbean Countercurrent (CCC). Other abbreviations refer to fronts: JMF: Jan Mayen Front, NCF: Norwegian Current Front, IFF: Iceland - Faroe Front, SAF: Subarctic Front, AF: Azores Front, ABF: Angola - Benguela Front, BCF: Brazil Current Front, STF: Subtropical Front, SAF: Subantarctic Front, PF: Polar Front, CWB/WGB: Continental Water Boundary / Weddell Gyre Boundary. Adapted from Duncan *et al*. (1982), Krauss (1986) and Peterson and Stramma (1991).

Benguela Current. The subpolar gyre of the northern hemisphere is modified by interaction with the Arctic circulation, to the extent that it is hardly recognizable as a gyre. It involves the North Atlantic Current, the Irminger Current, the East and West Greenland Currents, and the Labrador Current, with substantial water exchange with the Arctic Mediterranean Sea through the North Atlantic Current (and its extension into the Norwegian Current) and the East Greenland Current.

The Sverdrup relation performs particularly well near the equator, where geostrophic gradients are very small. It reveals the existence of an equatorial countercurrent between the North and South Equatorial Currents. As in the Pacific Ocean, this countercurrent flows down the Doldrums; but it is broader and less intense. This results from the reduced width of the Atlantic Ocean and from the fact that the Doldrums (or ITCZ) are not strictly zonal but angle across from Brazil to Sierra Leone, as mentioned earlier.

A notable discrepancy between Figures 4.4 and 4.5 or 4.6 is the failure of the wind-calculated pattern to reproduce the intense crowding of the contours of depth-integrated steric height off North America near Cape Hatteras (35°N). A similar failure occurs in the north-east Pacific Ocean, but it is not as severe there; in the Atlantic Ocean, the wind-calculated flow follows the coast to Labrador (50°N) before flowing east, whereas it in fact breaks away from the coast at Cape Hatteras (as indicated in the CTD-based flow field) and takes on the character of an intense jet.

The equatorial current system

As in the Pacific Ocean, the equatorial current system displays a banded structure when investigated in detail. Figure 14.3 is a schematic summary of all its elements as they occur in mid-year. The *Equatorial Undercurrent* (EUC) is the strongest, with maximum speeds exceeding 1.2 m s^{-1} in its core at about 100 m depth and transports up to 15 Sv. It is driven and maintained by the same mechanism as in the Pacific Ocean (see Chapter 8), strongest in the west and weakening along its path as a result of frictional losses to the surrounding waters. Observations show that it swings back and forth between two extreme positions 90 km either side of the equator at a rate of once every 2 - 3 weeks, while speed and transport oscillate between the maxima given above and their respective minima of 0.6 m s^{-1} and 4 Sv. The EUC was discovered by the early oceanographer John Young Buchanan during the *Challenger* expedition of 1872 - 1876 and described in 1886, but this discovery was forgotten until the discovery of the Pacific EUC in 1952 triggered a search for an analogous current in the Atlantic Ocean. CTD data reveal the presence of the EUC through the vertical spreading of isotherms in the thermocline (Figure 14.4); in the eastern Atlantic Ocean it can be seen as a prominent subsurface salinity maximum.

The three equatorial currents known from the depth-integrated circulation dominate the surface flow (Figure 14.3) and the hydrography (Figure 14.4; see Chapter 8 for a discussion of the relationship between thermocline slope and currents) but appear more complicated in detail. The *North Equatorial Current* (NEC) is a region of broad and uniform westward flow north of 10°N with speeds of 0.1 - 0.3 m s^{-1}. The eastward flowing *North Equatorial Countercurrent* (NECC, the countercurrent seen in the depth-integrated flow field) has similar speeds; it is highly seasonal and nearly disappears in February when the Trades in the northern hemisphere are strongest (Figure 14.5). The *South Equatorial Current*

(SEC), again a region of broad and uniform westward flow with similar speeds, extends from about 3°N to at least 15°S. Just as in the Pacific Ocean it is interspersed with eastward flow both at the surface and below the thermocline. The *South Equatorial Countercurrent* (SECC) is weak, narrow and variable and therefore not resolved by Figure 14.5, which is based on 2° averages in latitude. It often shows maximum speed (around 0.1 m s^{-1}) below 100 m depth and is masked by weak westward flow at the surface. The *North Equatorial Undercurrent* (NEUC) and the *South Equatorial Undercurrent* (SEUC) are both narrow and swift, with maximum speeds of 0.4 m s^{-1} near 200 m depth.
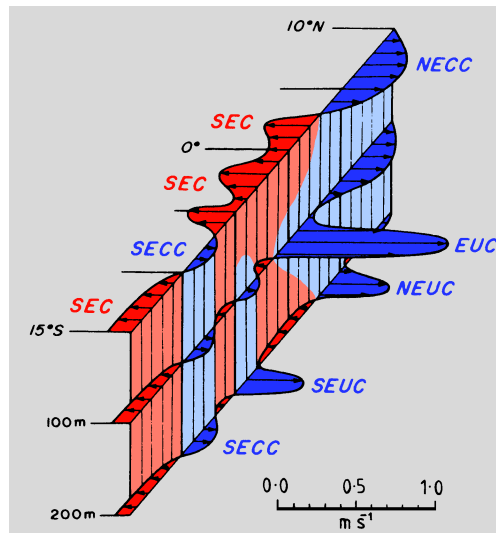
Fig. 14.3. A sketch of the structure of the equatorial current system during August. For abbreviations see text. After Peterson and Stramma (1991).
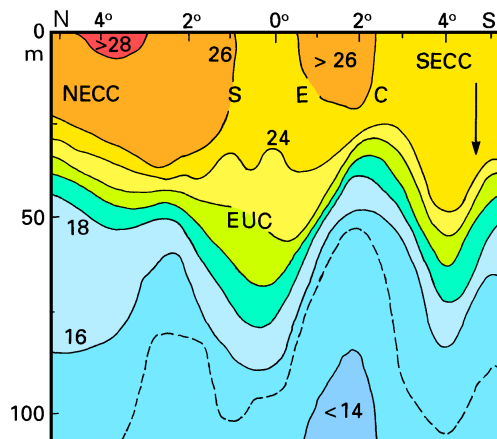

Fig. 14.4. Temperature section (°C) across the central part of the equatorial current system along 5°W. For abbreviations see text. Note the low surface temperature at the equator due to upwelling, the weakening of the thermocline in the EUC, and the poleward rise of the thermocline in the countercurrents. Adapted from Moore *et al*. (1978) .
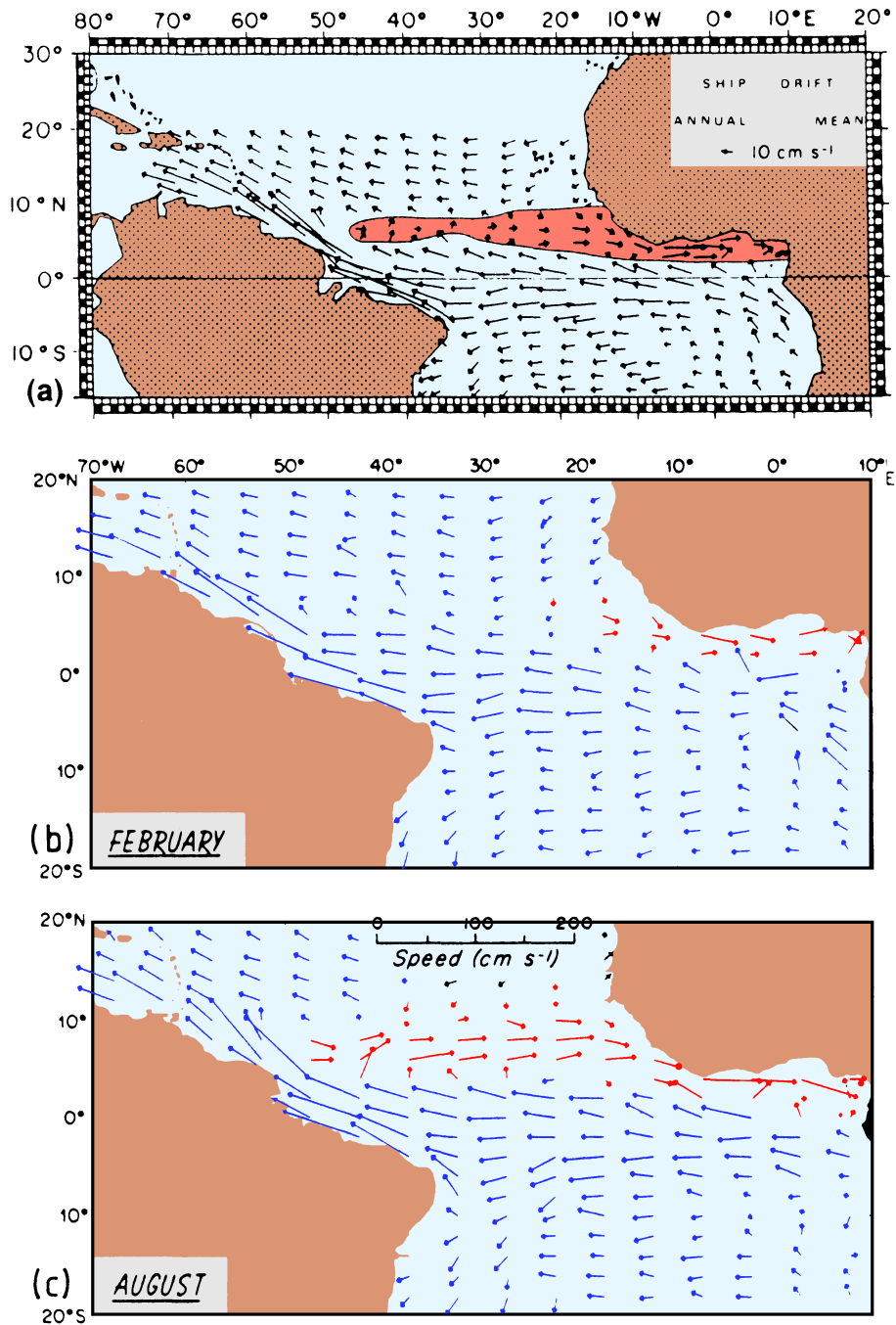
Fig. 14.5. Surface currents in the equatorial region as derived from ship drift data. (a) Annual mean, (b) February, (c) August. From Arnault (1987) and Richardson and Walsh (1986).

The most conspicuous feature of the equatorial circulation is the strong cross-equatorial transport along the South American coast in the *North Brazil Current*. Of the 16 Sv carried across 30°W in the South Equatorial Current during February/March, only 4 Sv are carried south into the Brazil Current while 12 Sv cross the equator (Stramma *et al.*, 1990). This is close to the estimated 15 Sv needed to feed the Deep Water source in the North Atlantic Ocean.

Little exchange between hemispheres occurs in the eastern part of the equatorial zone, the termination region of all eastward flow. The South Equatorial Countercurrent turns south, driving a cyclonic gyre centred at 13°S, 4°E which extends from just below the surface to at least 300 m depth with velocities approaching 0.5 m s^{-1} near the African coast where this relatively strong subsurface flow is known as the *Angola Current* (Figure 14.2). By opposing the northward movement of the Benguela Current it creates the Angola - Benguela Front, a feature seen in the temperature of the upper 50 m and in the salinity distribution to at least 200 m depth.
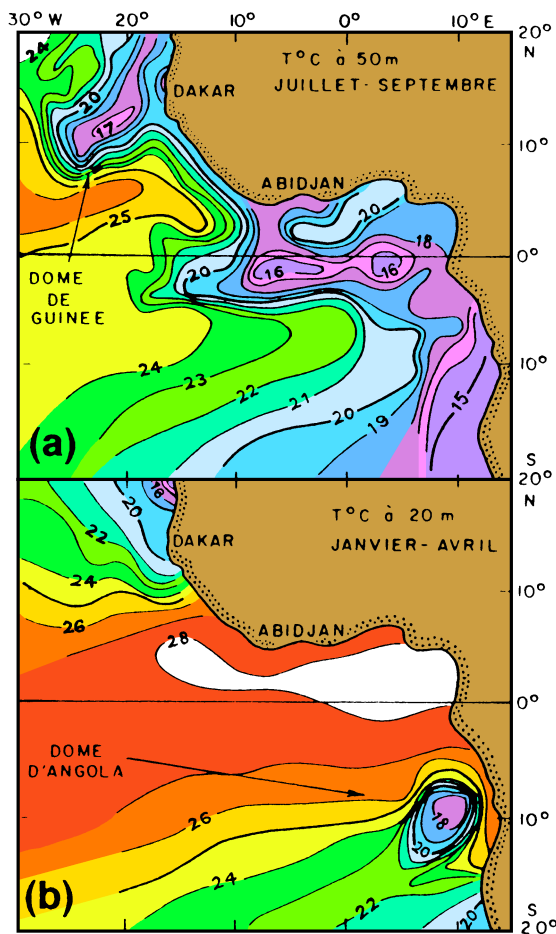

Fig. 14.6. The Angola Dome and the Guinea Dome as seen in temperature data from 20 m and 50 m depth. From Peterson and Stramma (1991)

The North Equatorial Countercurrent is prevented from flowing north by the east - west orientation of the coastline; it intensifies to an average 0.4 m s^{-1} along the Ivory Coast before its energy is dissipated in the Gulf of Guinea. However, some of its flow does escape north and combines with the North Equatorial Undercurrent to drive a small cyclonic gyre centred at 10°N, 22°W. A similar small gyre, centred near 10°S, 9°E and clearly distinct

from the larger gyre which incorporates the Angola Current, is driven by the South Equatorial Undercurrent. We know from our Rules 1, 1a, and 2 of Chapter 3 that cyclonic flow is accompanied by a sea surface depression and an elevation of the thermocline in the centre of the gyre (compare Figure 2.7, or Figures 3.3 and 3.4 which show the same rules operating in an anticyclonic gyre), so in a plot of temperature at constant depth the two gyres should show up as local temperature minima. Figure 14.6 proves that this is indeed the case but only in summer when the Trades of the respective hemisphere are weakest and the Undercurrents strongest. Because of the observed doming of the thermocline in summer the gyres are known as the *Angola* and *Guinea Domes*. The associated circulation exists throughout the year, although weaker in winter, and reaches to at least 150 m depth.

Western boundary currents

The Sverdrup calculation of Chapter 4 gave integrated volume transports for the Gulf Stream and the Brazil Current of 30 Sv. These numbers are modest in comparison to the results for the Kuroshio (50 Sv) or the Agulhas Current (70 Sv). They can be explained in part as reflecting the weakness of the Atlantic annual mean wind stress and the narrowness of the basin. However, they underestimate the Gulf Stream transport by a large margin. This failure of the Sverdrup calculation is a consequence of the recirculation of North Atlantic Deep Water. The westward intensification of all ocean currents influences the flow of Deep Water, too; so both the southward transport of Deep Water at depth and the north-ward flow of the recirculation below and above the thermocline are concentrated on the western side of the ocean. This adds some 15 Sv to the Gulf Stream transport in the upper 1500 m and subtracts the same amount from the transport of the Brazil Current. This large difference between the two major currents in the Atlantic Ocean does not come out in the vertically integrated flow (Figure 4.7), which shows complete separation of the oceanic gyres along the American coast near 12°S, 6°N, 18°N, and 50°N and similar transports for both boundary currents. This is true for the *wind-driven* component of the flow (i.e. excluding the Deep Water recirculation which is a result of thermohaline forcing), and it is correct when the flow is integrated over all depth, but it is misleading when taken as representative of the circulation in the upper ocean.

For these reasons, the strongest of the western boundary currents is the *Gulf Stream*, so called because it was originally believed to represent a drainage flow from the Gulf of Mexico. It has now been known for many decades that this is not correct and that the flow through the Strait of Florida stems directly from Yucatan Strait and passes the Gulf to the south. Even this flow constitutes only a portion of the source waters of the Gulf Stream. It turns out that it is better to speak of the Gulf Stream System and its various components, the Florida Current, the Gulf Stream proper, the Gulf Stream Extension, and its continuation as the North Atlantic and Azores Currents.

The *Florida Current* is fed from that part of the North Equatorial Current that passes through Yucatan Strait, with a possible contribution from the North Brazil Current (see below). In Florida Strait this current carries about 30 Sv with speeds in excess of 1.8 m s^{-1}. On average, the current is strongest in March, when it carries 11 Sv more than in November. Its transport is increased along the coast of northern Florida through input from the second path of the North Equatorial Current (the Antilles Current, see below).

Recirculation of Gulf Stream water in the Sargasso Sea increases its transport further. By the time the flow separates from the shelf near Cape Hatteras - a distance of 1200 km downstream - it has reached a transport of 70 - 100 Sv (much more than the 30 Sv suggested by the integrated flow calculation of Chapter 4). For the next 2500 km the *Gulf Stream* proper flows across the open ocean as a free inertial jet. Its transport increases initially through inflow from the Sargasso Sea recirculation region to reach a maximum of 90 - 150 Sv near 65°W. The current then begins to lose water to the Sargasso Sea recirculation, its transport falling to 50 - 90 Sv near the Newfoundland Rise (50°W, also known as the Grand Banks). Throughout its path current speed remains large at the surface and decreases rapidly with depth, but the flow usually extends to the ocean floor (Figure 14.7).
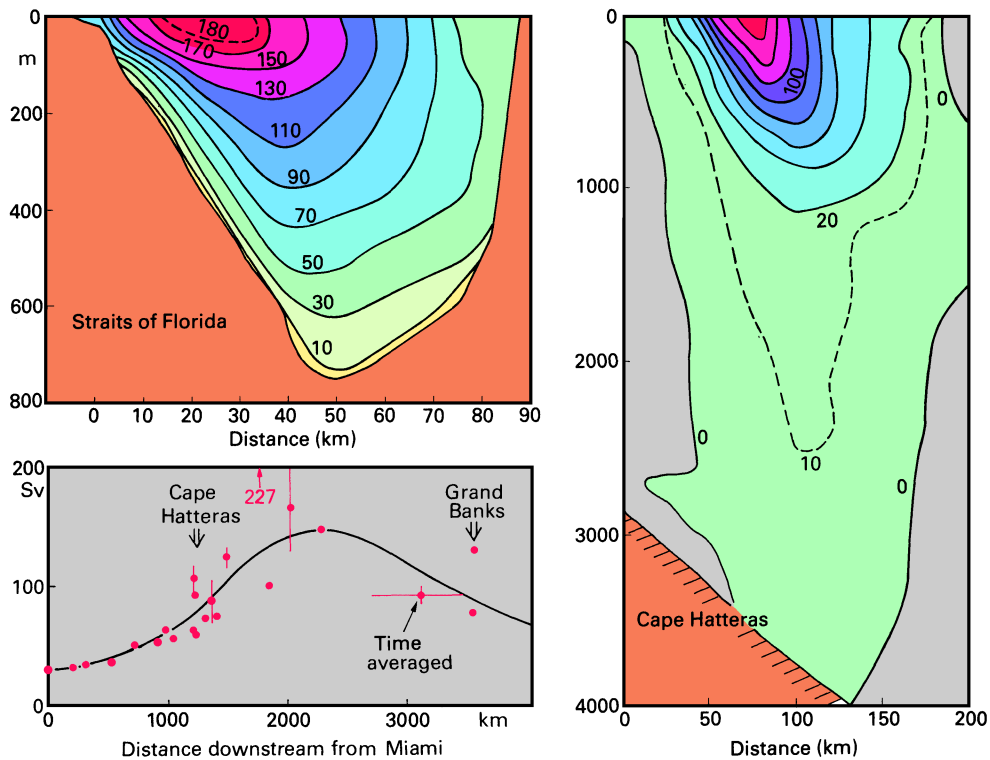

Fig. 14.7. A summary of Gulf Stream volume transports reported in the literature (based on Richardson (1985) and additional more recent data); and two sec–tions of annual mean velocity in the Florida Current and the Gulf Stream at Cape Hatteras, based on continuous vertical profiles of velocity from cruises over a 2 - 3   year period. Note the different depth and distance scales. From Leaman *et al*. (1989).

In the region east of 50°W, which is sometimes referred to as the Gulf Stream Extension, the flow branches into three distinctly different regimes (Figure 14.8). The *North Atlantic Current* continues in a northeastward direction towards Scotland and withdraws about 30 Sv

from the subtropical gyre, to feed the Norwegian Current and eventually contribute to Arctic Bottom Water formation. The *Azores Current* is part of the subtropical gyre; it carries some 15 Sv along 35 - 40°N to feed the Canary Current. The remaining transport does not participate in the ocean-wide subtropical gyre but is returned to the Florida Current and Gulf Stream via the much shorter path of the Sargasso Sea recirculation system.
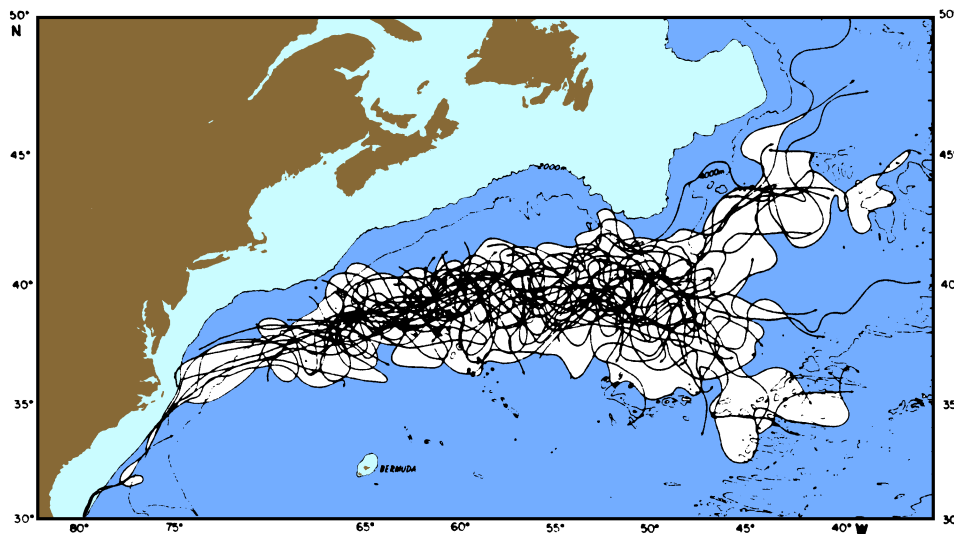

Fig. 14.8. Paths of satellite-tracked buoys in the Gulf Stream system. Most buoy tracks are from the period 1977 - 1981, some tracks going back to 1971. For clarity, only buoys with average velocity exceeding 0.5 m s^{-1} were used and loops indicative of meanders or eddies were removed. The branching of the Gulf Stream into the North Atlantic Current, Azores Current, and Sargasso Sea recirculation is visible in the tracks east of 55°W. From Richardson (1983a).

Free inertial jets which penetrate into the open ocean become unstable along their path. They form meanders which eventually separate as eddies. Meanders which separate poleward of the jet develop into anticyclonic (warm-core) eddies, those separating equatorward produce cyclonic (cold-core) eddies (Figure 14.9). Because of their hydrographic structure - a ring of Gulf Stream water with velocities comparable to those of the Gulf Stream itself, isolating water of different properties from the surrounding ocean - these eddies are often referred to as rings. Most of the Gulf Stream rings are formed in the Gulf Stream Extension region and move slowly back against the direction of the main current (Figure 14.10). Rings formed north of the Gulf Stream are restricted in their movement and often merge with the main flow after a short journey eastward; but the cold-core eddies to the south dominate the Sargasso Sea recirculation region, where some 10 rings can be found at any particular time. Satellite images of sea surface temperature such as Figure 14.11 display them as isolated regions of warm water north of the Gulf Stream and regions of cold water to the south. In the world map of eddy energy (Figure 4.8) the Sargasso Sea recirculation region stands out as one of the most energetic.
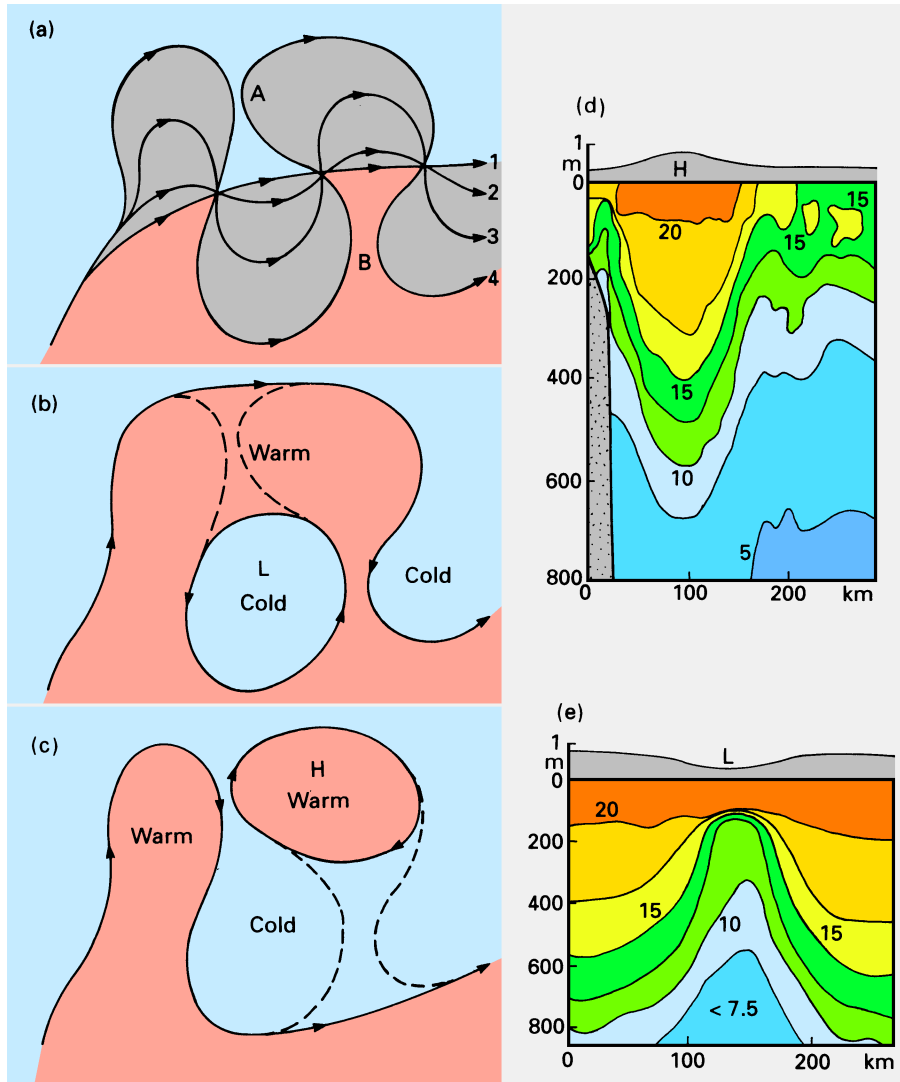
Fig. 14.9. A sketch of eddy formation in a free inertial jet and the associated hydrographic structure. (a) Path of the jet at succesive times 1 - 4. (b) A cyclonic (cold-core) ring formed after merger of the path at location *A*. The open line is the Gulf Stream path after ring formation, the closed line the ring, the dotted line the path just before eddy formation. (c) A similar representation of an anticyclonic (warm-core) ring formed if the jet merges at location *B* instead. *H* and *L* indicate high and low pressure. (d) A temperature section (°C) through an anticyclonic ring. (e) A section through a cyclonic ring. The shape of the sea surface shown in (d) and (e) was not measured but follows from Rules 1, 1a, and 2 of Chapter 3. Panels (a) - (c) show a northern hemisphere jet; the situation in the southern hemisphere is the mirror image with respect to the equator. Panels (d) and (e) apply to both hemispheres; they are adapted from Richardson (1983b).
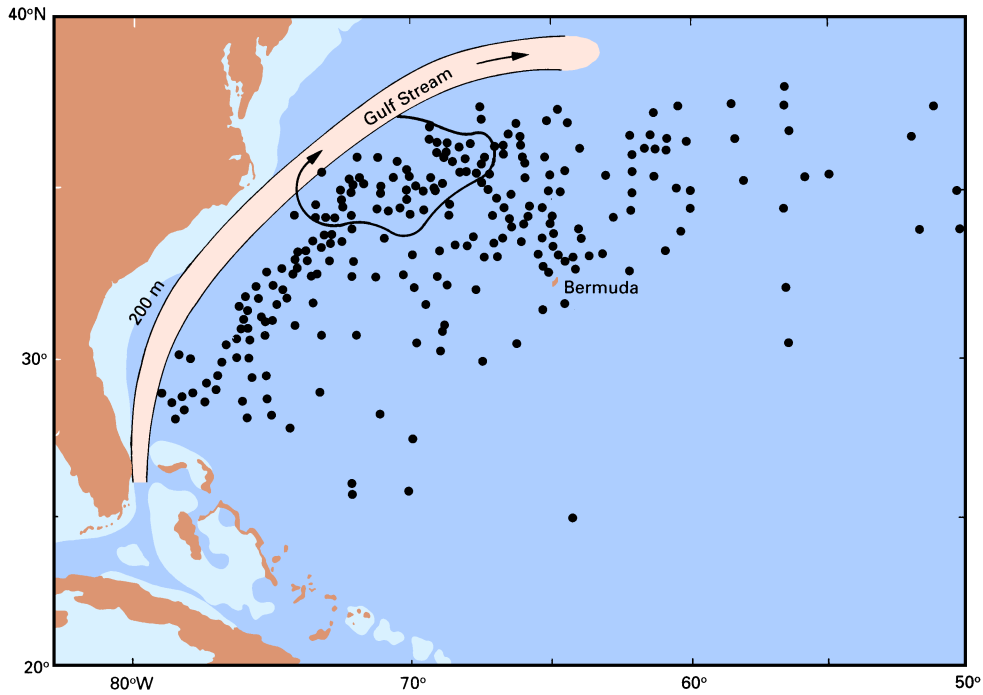
Fig. 14.10. Geographical distribution of 225 cold-core rings reported for the period 1932 - 1983. Ring movement is generally towards the southwest until the rings decay or are absorbed again into the Gulf Stream. The arrow, the path of a ring observed in 1977, gives an example of typical ring movement. Adapted from Richardson (1983b).
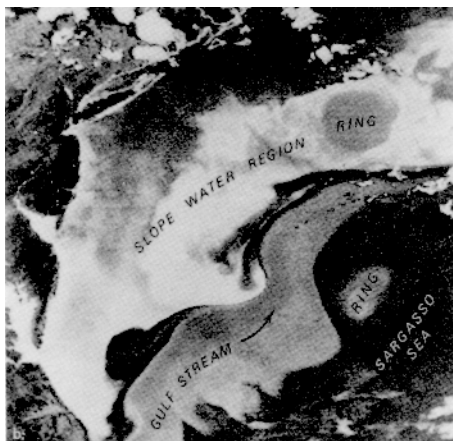

Fig. 14.11. Infrared satellite image of the Gulf Stream System. The Gulf Stream is seen as a band of warm water between the colder Slope Water region and the warmer Sargasso Sea. Two rings can be seen; both contain water of Gulf Stream temperature, but the northern ring is of the warm-core type and has anti-cyclonic rotation, while the ring in the south is a cold-core ring with cyclonic rotation. The region shown covers approximately
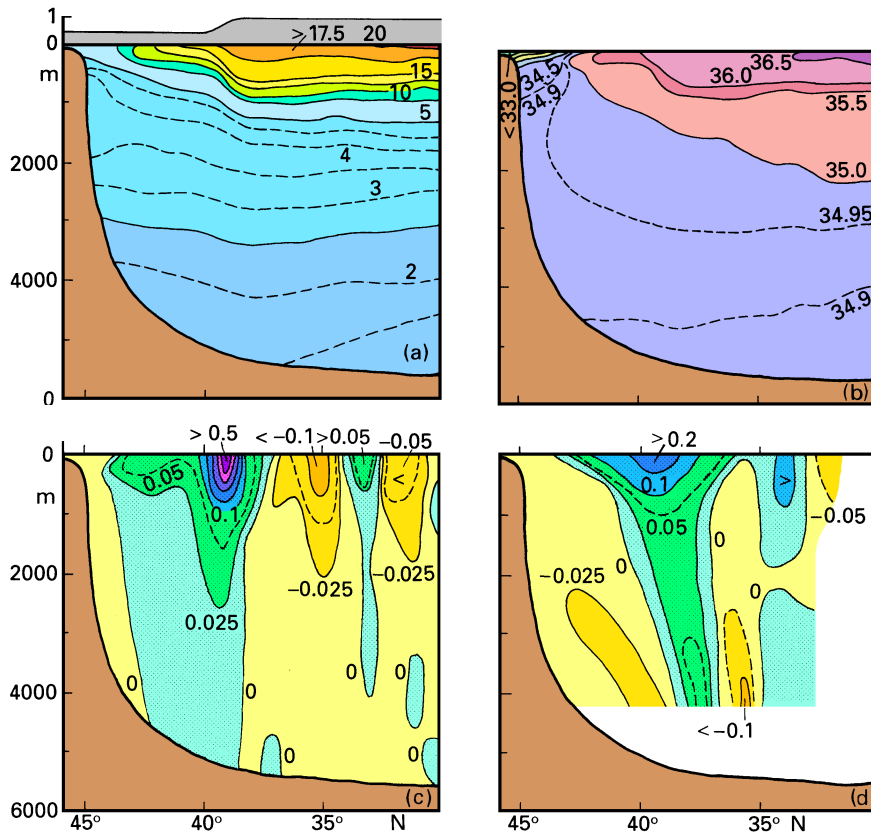
Fig. 14.12. A section through the Gulf Stream and its countercurrents across 55°W. (a) Potential temperature (°C) and sea level (m), (b) salinity, (c) geostrophic current (m s^{-1}) relative to the sea floor, (d) mean current (m s^{-1}) as derived from a combination of drifters, subsurface floats, and current meter moorings. The sections are based on data from 8 cruises between 1959 - 1983. From Richardson (1985). The shape of the sea surface as seen in more recent satellite altimeter observations is sketched above the temperature panel.

Most transport estimates for the Gulf Stream are based on geostrophic calculations which, according to our Rule 2 in Chapter 3, should be accurate to within 20%. The associated pressure gradient is maintained by a drop in sea level across the current of some 0.5 m towards the coast and, according to our Rule 1a, a corresponding thermocline rise of about 500 m. This is demonstrated by Figure 14.12 which also reveals the existence of two countercurrents, one inshore - between the continental slope and the Gulf Stream - and one offshore, as part of the long-term mean situation. Actual velocities at any particular time can be much larger, since the strong currents in the rings disappear in the mean and variability in the position of the Gulf Stream acts to reduce the peak velocity in the mean as well. Observed peak velocities usually exceed 1.5 m s^{-1}.The Gulf Stream is an

important heat sink for the ocean. Net annual mean heat loss, caused by advection of cold dry continental air from the west, exceeds 200 W m^{-2} (Figure 1.6). A brief period of net heat gain occurs from late May to August when warm saturated air is advected from the south (Figure 1.2).

The *Labrador Current* is the western boundary current of the subpolar gyre. This gyre receives considerable input of Arctic water from the East Greenland Current. Measurements south of Cape Farewell indicate speeds of 0.3 m s^{-1} on the shelf and above the ocean floor at depths of 2000 - 3000 m and 0.15 m s^{-1} at the surface, for the combined flow of the East Greenland and Irminger Currents. Transport estimates for the Irminger Current amount to 8 - 11 Sv. Even if this is combined with the estimated 5 Sv for the East Greenland Current of Chapter 7, it does not explain the 34 Sv derived by Thompson *et al*. (1986) for the West Greenland and Labrador Currents from hydrographic section data. Substantial recirculation must therefore occur in the Labrador Sea if these estimates are correct. Earlier estimates of 10 Sv or less were based on geostrophic calculations with 1500 m reference depth, clearly not deep enough for western boundary currents which extend to the ocean floor. The Labrador Current is strongest in February when on average it carries 6 Sv more water than in August. It is also more variable in winter, with a standard deviation of 9 Sv in February but only 1 Sv in August.
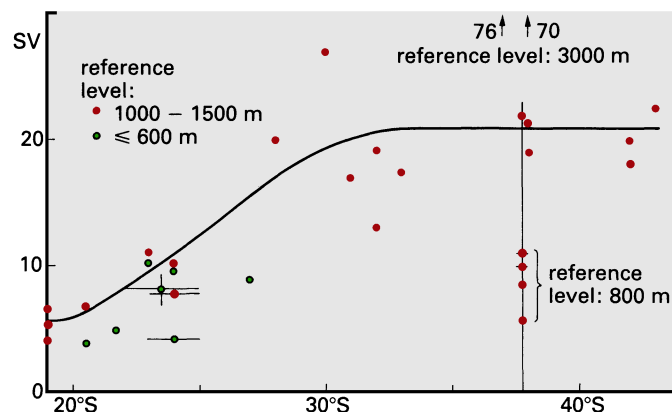

Fig. 14.13. A summary of Brazil Current transports reported in the literature. Unless indicated otherwise, transports assume a level of no motion between 1000 m and 1500 m. After Peterson and Stramma (1991).

The western boundary current of the south Atlantic subtropical gyre, the *Brazil Current*, begins near 10°S with a trickle of 4 Sv supplied by the South Equatorial Current. Over the next 1500 km its strength increases to little more than 10 Sv through incorporation of water from the recirculation region over the Brazil Basin. The current is comparatively shallow, nearly half of the flow occurring on the shelf with the current axis above the 200 m isobath. In deeper water northward flow of Antarctic Intermediate Water is embedded in the Current at intermediate depths (below 400 m). A well-defined recirculation cell south

of the Rio Grande Rise (the analogy to the Sargasso Sea recirculation regime of the Gulf Stream) leads to an increase in transport to 19 - 22 Sv near 38°S (Figure 14.13), which corresponds to a rate of increase comparable to that observed in the Gulf Stream. All these estimates are derived from geostrophic calculations with levels of no motion near or above 1500 m and therefore do not include the considerable transport of North Atlantic Deep Water below. More recent estimates which use 3000 m as level of no motion give total transports of 70 - 76 Sv near 38°S (Peterson and Stramma, 1991). The difference is larger than can be explained by the transport of Deep Water and indicates that significant recirculation must occur in the south Atlantic Ocean below 1500 m depth.
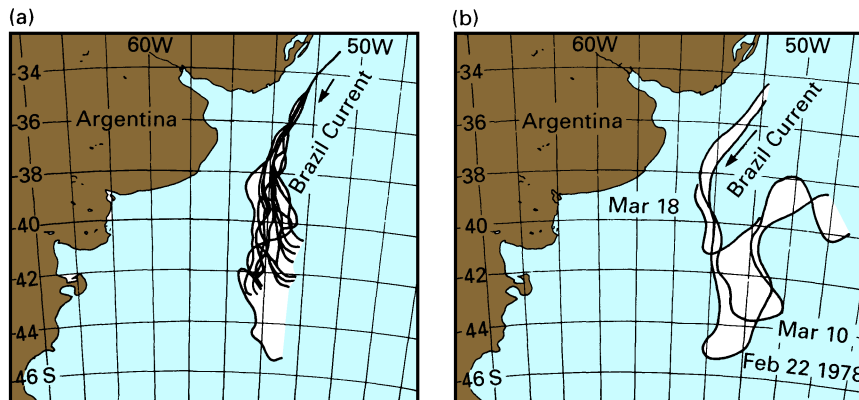

Fig. 14.14. The separation region of the Brazil Current. (a) mean position of the Brazil Current as indicated by the position of the thermal front between the Brazil and Malvinas Currents during September 1975 - April 1976; (b) a succession of three positions of the thermal front, indicating northward retreat of the Brazil Current. Two eddies formed between 22 February and 18 March; they are not included here. From Legeckis and Gordon (1982).

The Brazil Current separates from the shelf somewhere between 33 and 38°S, forming an intense front with the cold water of the *Malvinas Current*, a jet-like northward looping excursion of the Circumpolar Current also known as the Falkland Current (Figure 14.14). The separation point is more northerly during summer than winter, possibly as part of a general northward shift of the subtropical gyre in response to the more northern position of the atmospheric high pressure system (Figure 1.3) and northward movement of the contour of zero curl(τ/f) during summer (December - February). The southernmost extent of the warm Brazil Current after separation from the shelf varies between 38°S and 46°S on times scales of two months and is linked with the formation of eddies, the mechanism being very similar to that of the East Australian Current (Figure 14.15; see also Figure 8.19). Observed current speeds in Brazil Current eddies are near 0.8 m s^{-1}; transport estimates are in the vicinity of 20 Sv. Most eddies escape from the recirculation region and are swept eastward with the *South Atlantic Current*. This can be seen in the distribution of eddy energy of Figure 4.8; the large area of high eddy energy centred on 40°S, 52°W corresponds to the region of eddy formation, its tail along 48°S to the path of the decaying eddies. The

two separate regions of high eddy energy east of South America also indicate that the South Atlantic and Circumpolar Currents are clearly different regimes. Geostrophic determinations of zonal transport east of 10°W between 30°S (the centre of the subtropical gyre) and 60°S invariably indicate a transport minimum near 45°S, indicating a separation zone between the South Atlantic and Circumpolar Currents. Fig. 14.15. Infrared satellite images of the Brazil Current separation obtained in October 1975 (left) and January 1976 (right). Dark is warm, light is cold; numbers show temperatures in °C. A recently formed eddy with a temperature of 18°C is seen in January 1976 south of the Brazil Current. From Legeckis and Gordon (1982).
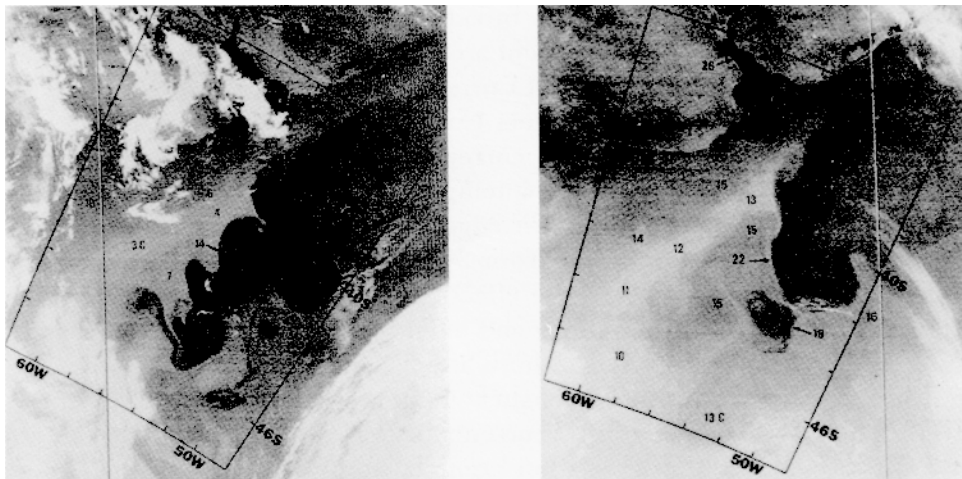

Fig. 14.15. Infrared satellite images of the Brazil Current separation obtained in October 1975 (left) and January 1976 (right). Dark is warm, light is cold; numbers show temperatures in °C. A recently formed eddy with a temperature of 18°C is seen in January 1976 south of the Brazil Current. From Legeckis and Gordon (1982).

Before concluding this section we mention the *North Brazil Current* and *Guyana Current* as another western boundary current system of the Atlantic Ocean. From the point of view of North Atlantic Deep Water recirculation it would be pleasing to see both as elements of continuous northward flow in and above the thermocline which starts at 16°S in the South Equatorial Current and continues through the American Mediterranean Sea to 27°N, eventually feeding into the Florida Current. Although this current system has received much less attention than is warranted by its important role in the global transport of heat, it is fair to say that the continuity of northward flow at the surface is questionable. There is no doubt about the existence of the North Brazil Current; observed surface speeds in excess of 0.8 m s^{-1} testify for its character as a jet-like boundary current. The character of the Guyana Current is much more obscure; eddies related to flow instability have been reported, but some researchers doubt whether the Guyana Current exists as a permanent current. There has also been some documentation (Duncan *et al*., 1982) that the Antilles Current is not identifiable as a permanent feature of the circulation and may indeed not exist as a

continuous current. Since the flow from the North Equatorial Current has to reach the Florida Current somehow, net mean movement in both the Guyana and Antilles Currents has to be toward northwest. The topic will be taken up again in the discussion of the American Mediterranean Sea in Chapter 16.

Eastern boundary currents and coastal upwelling

South of 45°N the circulation in the eastern part of the Atlantic Ocean has many similarities with that of the eastern Pacific Ocean. In the northern hemisphere the Canary Current is a broad region of moderate flow where the temperate waters of the Azores Current are converted into the subtropical water that feeds into the North Equatorial Current. In the southern hemisphere the same process occurs in the Benguela Current. Both currents are therefore characterized, when compared with currents in the western Atlantic Ocean at the same latitudes, by relatively low temperatures. As in the Pacific Ocean, equatorward winds along the eastern edge of the ocean, from Cape of Good Hope to near the equator and from Spain to about 10°N, increase the temperature contrast by adding the effect of coastal upwelling. Although the currents associated with the upwelling and those which constitute the recirculation in the subtropical gyres further offshore are dynamically independent features, the names Canary Current and Benguela Current are usually applied to both. As in other eastern ocean basins, currents in the eastern Atlantic Ocean are dominated by geostrophic eddies (an example from the vicinity of the Canary Current region is shown in Figure 4.9). Current reversals caused by passing eddies are common.

The dynamics of coastal upwelling were discussed in Chapter 8, so it is sufficient here to concentrate on regional aspects and identify the various elements of coastal upwelling systems in the Atlantic context. The *Benguela Current* upwelling system (Figure 14.16) is the stronger of the two, lowering annual mean sea surface temperatures to 14°C and less close to the coast - two degrees and more below the values seen in Figure 2.5 near the coast which indicate the effect of equatorward flow in the subtropical gyre. It is strongest in the south during spring and summer when the Trades are steady; during winter (July - September), it extends northward but becomes more intermittent because the Trades, although stronger, are interrupted by the passage of eastward travelling atmospheric lows. The width of the upwelling region coincides with the width of the shelf (200 km). Velocities in the equatorward surface flow are in the range $0.05 - 0.20$ m s^{-1}; in the coastal jet near the shelf break they exceed 0.5 m s^{-1}. Poleward flow occurs on the shelf above the bottom and over the shelf break with speeds of $0.05 - 0.1$ m s^{-1}, advecting oxygen-poor water from the waters off Angola; the resulting oxygen minimum along the slope can be observed over a distance of 1600 km to 30°S. The interface between equatorward surface movement and poleward flow underneath often reaches the surface on the inner shelf, producing poleward flow along the coast.

Further offshore beyond the shelf break, the equatorward surface layer flow merges with the equatorward transport of thermocline water in the Benguela Current, while poleward movement above the ocean floor continues uninterrupted, feeding into the cyclonic circulation of the deeper waters discussed in the next chapter. The dynamic independence of the recirculation in the subtropical gyre and the coastal upwelling is seen in the fact that the Benguela Current gradually leaves the coast between 30°S and 25°S, while the upwelling

reaches further north to Cape Frio (18°S). Geostrophic transport in the gyre circulation relative to 1500 - 2000 m depth is estimated at 20 - 25 Sv. This compares with a maximum of 7 Sv in the jet of the upwelling system (Peterson and Stramma, 1991).
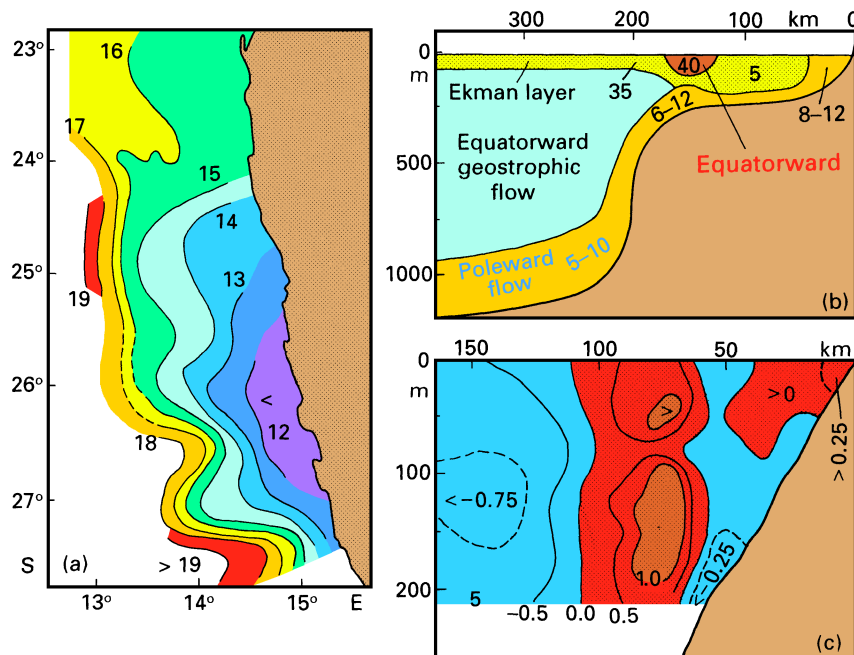

Fig. 14.16. The Benguela Current upwelling system. (a) Sea surface temperature (°C) in the northern part as observed during February 1966. (b) Sketch of the mean circulation. Transverse flow occurs in the bottom and Ekman layers; average speeds are given in cm s^{-1}, westward flow is shaded. Major alongshore (poleward or equatorward) flows are also indicated. (c) Observations of the equatorward jet (m s^{-1}, northward flow is shaded) from January 1973 in the south near 34°S. Adapted from Bang (1971), Nelson (1989), and Bang and Andrews (1974).

Strong seasonal variability and large contrast between the waters in the north and south are the main characteristics of the *Canary Current* upwelling system. Although the width of the upwelling region is narrow (less than 100 km), it exceeds the width of the shelf in most places. Observations on the shelf, which on average is only 60 - 80 m deep, show an unusually shallow Ekman layer at the surface with offshore movement extending to about 30 m depth, an intermediate layer of equatorward geostrophic flow, and a bottom layer with onshore flow (Figure 14.17c). An equatorward surface jet occurs just inshore of the shelf edge, while the undercurrent is usually restricted to the continental slope (Figure 14.17b). Velocities in all components of the current system are similar to those reported from the Benguela Current upwelling system.

The Canary Current upwelling reaches its southernmost extent in winter when the Trades are strongest (Figure 14.18). It then extends well past Cap Blanc, the separation point of the Canary Current from the African coast (Figure 14.2).
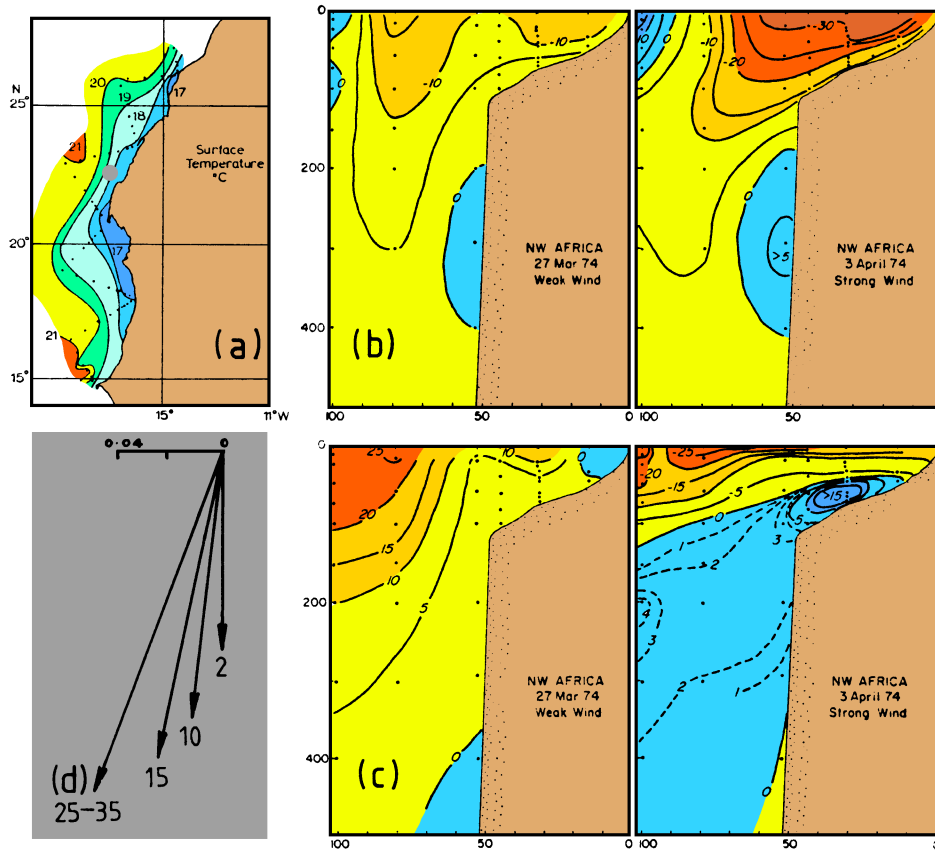
Fig. 14.17. The Canary Current upwelling system. (a) Sea surface temperature (°C) as observed in April/May 1969; (b) alongshore and (c) onshore velocities (cm s^{-1}, positive is northward and eastward) during periods of weak and strong wind, (d) observed mean velocities over a 29 day period at the position indicated by the dot in panel (a), in 74 m water depth; numbers indicate distance from the bottom. Note the alignment of the current at mid-depth with the direction of the coast, and the shoreward turning of the current as the bottom is approached. From Hughes and Barton (1974), Huyer (1976), and Tomczak and Hughes (1980).

The boundary between the westward turning Canary Current and the cyclonic circulation around the Guinea Dome marks the boundary between North Atlantic Central Water and South Atlantic Central Water, the water masses of the thermocline (which will be discussed in detail in Chapter 15). Low salinity South Atlantic Central Water is transported poleward with the surface current found along the coast of Mauritania. The undercurrent of the upwelling circulation is the continuation of this surface current. During summer when upwelling is restricted to the region north of Cap Blanc (21°N), poleward flow dominates the surface and subsurface layers south of Cap Blanc offshore and inshore; during winter it is restricted to subsurface flow along the continental slope. The depth of the undercurrent

increases along its way to 300 - 600 m off Cape Bojador (27°N). In hydrographic observations it is evident as a salinity minimum caused by its high content of South Atlantic Central Water (Figure 14.19).
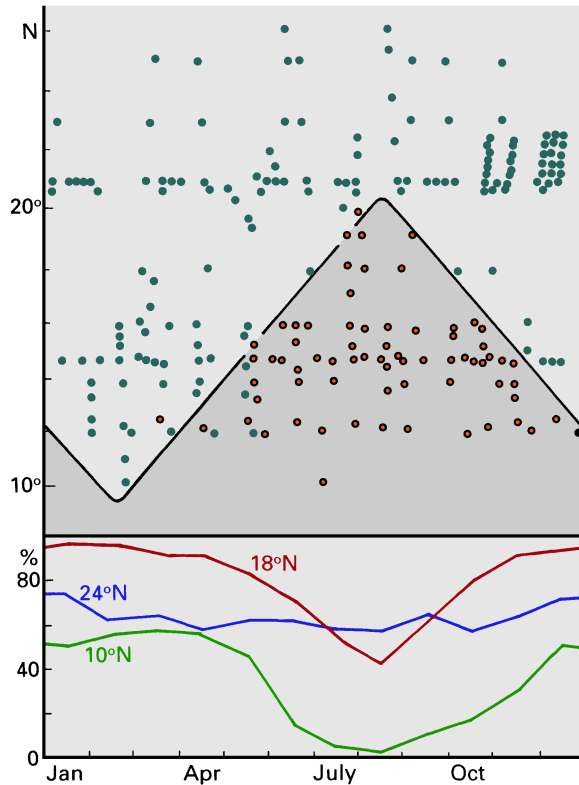

Fig. 14.18. Seasonal variability of the Canary Current upwelling system.

(a) southern boundary of the upwelling region; full dots indicate observed up-welling, circled dots indicate observed absence of upwelling.

(b) frequency of occurrence of winds favorable for upwelling (wind direction is in the quarter between alongshore toward south and exactly offshore). Adapted from Schemainda *et al*. (1975).

A rather unique coastal upwelling region is found along the coasts of Ghana and the Ivory Coast where the African continent forms some 2000 km of zonally oriented coastline. Winds in this region are always very light and never favorable for upwelling. The sea surface temperature, however, is observed to drop regularly by several degrees, for periods of 14 days during northern summer (Figure 14.20). These temperature variations are coupled with reversals of the currents on the shelf, periodic lifting of the thermocline, and advection of nutrient-rich water towards the coast. The upwelling, which is clearly not related to local wind conditions, is caused by variations in the wind field over the *western* equatorial Atlantic Ocean which produce wave-like disturbances of the thermocline in the equatorial region known as Kelvin waves. Equatorial Kelvin waves are a major component of interannual variations in the circulation of the Pacific Ocean; a detailed discussion of their dynamics is therefore included in Chapter 19. For the purpose of the present discussion it is sufficient to note that they consist of a series of depressions and bulges of the thermocline, move eastward along the equator at about 200 km per day, and when reaching the eastern

coastline continue poleward. The progression of the thermocline bulges and depressions is of course linked with significant horizontal transport of water, i.e. variations in the currents.

In the Atlantic Ocean, equatorial Kelvin waves generated off the coast of Brazil reach the Gulf of Guinea in little more than one month. They continue northward and then eastward along the African coast where they are recorded as strong regular upwelling events. For the local fishery they are of great importance, since they replenish the coastal waters with nutrients by lifting the nutrient-rich waters of the oceanic thermocline onto the shelf.

Fig. 14.19. (Left) The undercurrent of the Canary Current upwelling system as seen in hydrographic observations.

(a) a salinity section along the continental slope, showing saline North Atlantic Central Water north and low salinity South Atlantic Central Water south of 20 - 22°N and the salinity anomaly on the $\sigma_{\Theta}= 26.8$ density surface (thin dotted line) caused by advection of SACW,

(b) distribution of water masses in a section across the shelf and slope at 25°N, expressed as % NACW content (SACW content is 100 - %NACW),

(c) a similar section at 21°N. The data for (a) were collected in April 1969, the data for (b) and (c) in February 1975. Note that the undercurrent is already well submerged at 21°N during 1969 but still close to the surface at 21°N in 1975.

Adapted from Hughes and Barton (1974) and Tomczak and Hughes (1980).
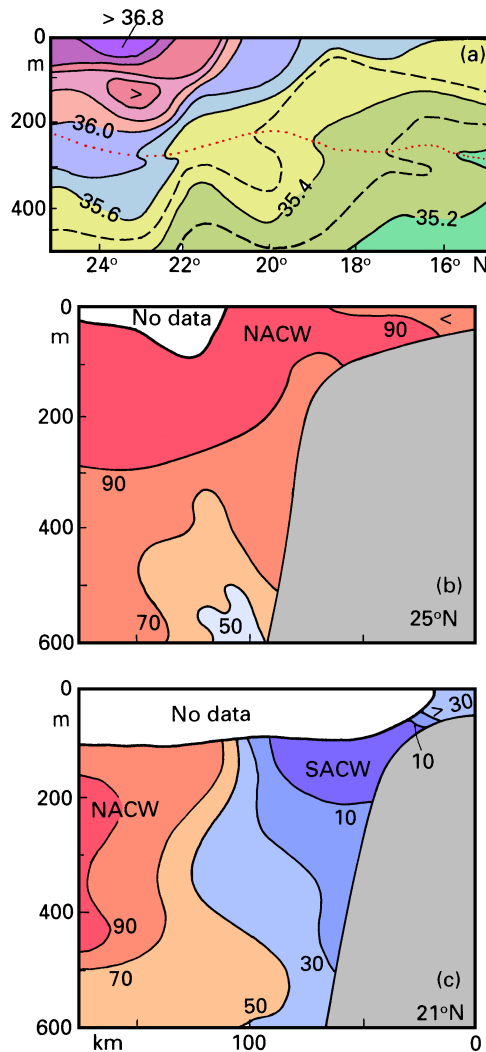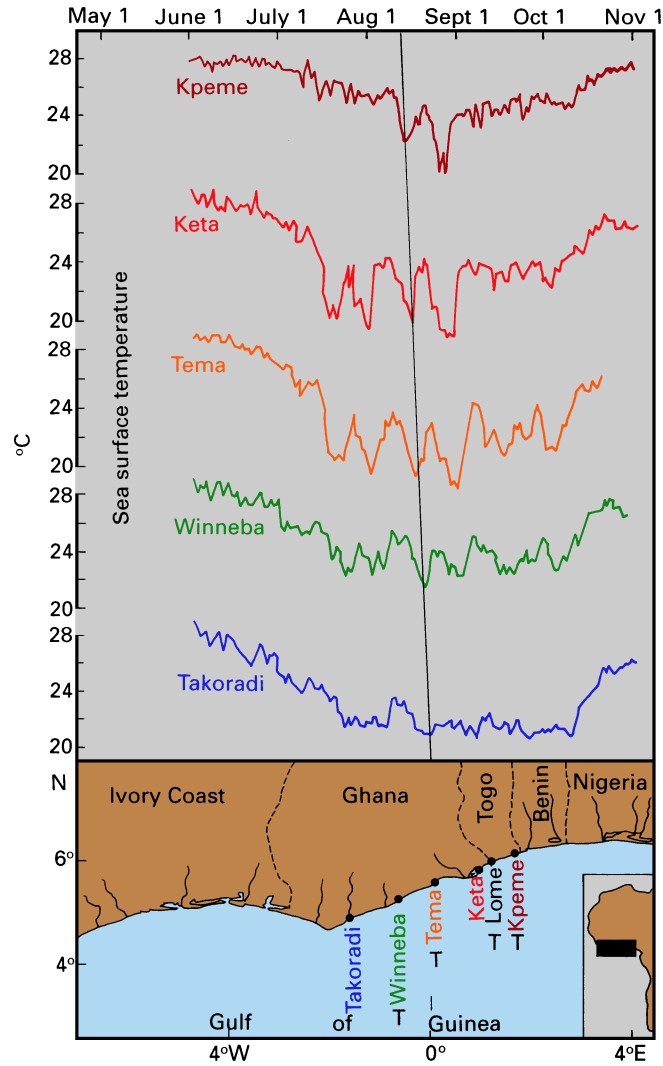
Fig. 14.20. (Right) Sea surface temperature (°C) as observed in 1974 at various locations in the Gulf of Guinea, showing periodic upwelling caused by waves of 14 day period during summer. Note the westward propagation indicated by the tilt of the line through the temperature minima. Adapted from Moore *et al.* (1978).